

Resource-Optimized Fermionic Local-Hamiltonian Simulation on Quantum Computer for Quantum Chemistry

Qingfeng Wang,^{1,*} Ming Li,^{2,†} Christopher Monroe,^{2,3,‡} and Yunseong Nam^{2,§}

¹*Chemical Physics Program and Institute for Physical Science and Technology,
University of Maryland, College Park, MD 20742, USA*

²*IonQ, College Park, MD 20740, USA*

³*Joint Quantum Institute, Department of Physics,
and Joint Center for Quantum Information and Computer Science,
University of Maryland, College Park, MD 20742, USA*

(Dated: June 3, 2022)

Abstract

The ability to simulate a fermionic system on a quantum computer is expected to revolutionize chemical engineering, materials design, nuclear physics, to name a few. Thus, optimizing the simulation circuits is of significance in harnessing the power of quantum computers. Here, we address this problem in two aspects. In the fault-tolerant regime, we optimize the R_z gate counts and depths, assuming the use of a product-formula algorithm for implementation. In the pre-fault tolerant regime, we optimize the two-qubit gate counts, assuming the use of variational quantum eigensolver (VQE) approach. Specifically to the latter, we present a framework that enables bootstrapping the VQE progression towards the convergence of the ground-state energy of the fermionic system. This framework, based on perturbation theory, also improves the energy estimate at each cycle of the VQE progression dramatically, resulting in significant savings of quantum resources required to be within a pre-specified tolerance from the known ground-state energy in the test-bed, classically-accessible system of the water molecule. We also explore a suite of generalized transformations of fermion to qubit operators and show that resource-requirement savings of up to nearly 20% is possible.

PACS numbers: 03.67.Ac, 03.67.Lx

* keewang@umd.edu

† li@ionq.co

‡ monroe@umd.edu

§ nam@ionq.co

I. INTRODUCTION

Simulating fermionic matters on a quantum computer has recently been receiving much attention. Already available in the literature are various chemistry and nuclear physics simulation results [1–6], performed across multiple quantum computing platforms, including superconducting [1, 3, 5] and trapped-ion [2, 4, 6] based approaches. The limelight on the simulation of fermionic systems on a quantum computer is not accidental. Simulations of these systems are useful for furthering fundamental science and practical engineering [7, 8], and quantum computers are expected to enable the quantum simulations of fermions undergoing local interactions [9, 10], a task believed to be classically difficult to scale.

Broadly speaking, simulations of fermionic systems on a quantum computer may be classified into two categories: a variational, quantum-classical hybrid simulation [11], suitable for imperfect, pre-fault tolerant (pre-FT) quantum computers, and a Hamiltonian dynamics simulation based on pure quantum simulation algorithms [12], typically considered in fault-tolerant (FT) quantum computers. In the context of estimating the ground-state energy of a fermionic system, the former leverages efficient preparation of ansatz states and evaluation of operator expectation values, both enabled by quantum computers. The latter leverages the ability of a quantum computer to efficiently simulate evolution of quantum systems with a local Hamiltonian, which, when combined with quantum phase estimation [13], allows us to evaluate the ground-state energy of the system.

In the pre-FT regime, quantum computational cost is dominated by the use of multi-qubit gates. In the FT regime, where quantum circuits are typically composed of gates in the Clifford+T gateset, quantum computational cost is dominated by the use of $T := \begin{pmatrix} 1 & 0 \\ 0 & e^{i\pi/4} \end{pmatrix}$ gates, many of which are used in the FT implementation of $R_z(\theta) := \begin{pmatrix} e^{-i\theta/2} & 0 \\ 0 & e^{i\theta/2} \end{pmatrix}$ gates (see, e.g., [14]). In this paper, we present approaches that optimize quantum simulations of fermionic systems in either the pre-FT regime, reducing the number of multi-qubit gates, or in the FT regime, reducing the number of R_z gates or the number of time steps that R_z gates need to be applied, in the simulation circuit.

Our paper is structured as follows. In Sec. II we briefly define the scope of the problem in both the pre-FT and the FT regimes. In Sec. III, we present methods to optimize FT quantum simulations on the level of explicit circuit construction. In Sec. IV, we show two complementary approaches that result in quantum resource savings in pre-FT regime, i.e., a second-order perturbation based approach and a generalized fermion to qubit operator transformation. We discuss our results in Sec. V and conclude in Sec. VI.

II. PROBLEM

We consider in this paper, as a concrete example, a fermionic system evolving according to a time-independent, local, second-quantized Hamiltonian H in the occupation basis

$$H = \sum_{p,q} h_{pq} a_p^\dagger a_q + \sum_{p,q,r,s} h_{pqrs} a_p^\dagger a_q^\dagger a_r a_s, \quad (1)$$

where a_p^\dagger and a_q denote the fermionic creation and annihilation operators on the p th and q th levels, respectively, and h_{pq} and h_{pqrs} denote single- and double-fermion Hamiltonian coefficients, respectively. The fermionic operators follow the canonical anti-commutation

relations

$$\{a_j, a_k\} = 0, \quad \{a_j^\dagger, a_k^\dagger\} = 0, \quad \{a_j, a_k^\dagger\} = \delta_{jk} \mathbf{1}, \quad (2)$$

where $\{A, B\}$ denotes the anti-commutator $AB + BA$, δ_{jk} is a Kronecker delta, and $\mathbf{1}$ is an identity operator. For their implementations on a quantum computer, the fermionic operators need to be suitably transformed [15–17]. A well-known, popular choice is the Jordan-Wigner (JW) transformation [15], defined for a n -qubit system according to

$$a_j^\dagger = 1^{\otimes n-j-1} \otimes \sigma_+ \otimes \sigma_z^{\otimes j}, \quad a_j = 1^{\otimes n-j-1} \otimes \sigma_- \otimes \sigma_z^{\otimes j}, \quad (3)$$

where $j \in [0, n-1]$, \otimes denotes tensor product, $\sigma_+ := \begin{pmatrix} 0 & 0 \\ 1 & 0 \end{pmatrix}$, $\sigma_- := \begin{pmatrix} 0 & 1 \\ 0 & 0 \end{pmatrix}$, and $\sigma_z := \begin{pmatrix} 1 & 0 \\ 0 & -1 \end{pmatrix}$.

In the case where we consider a quantum dynamics simulation approach more suitable for the FT regime, we aim to implement the evolution operator $U_{\text{evo}} = e^{-iHt}$ on a quantum computer, where H is the system Hamiltonian and t is the duration by which we desire to evolve the system forward in time. A host of algorithms that (approximately) implement U_{evo} have been proposed, such as the asymptotically optimal quantum signal processing [18, 19]. However, it has been shown that for certain Hamiltonians including ones of the form (1) a more straightforward technique of the $2k^{\text{th}}$ order product formula (PF) can be implemented more efficiently in practice [12, 20]. Thus in this paper we choose the PF algorithm for the FT regime quantum simulation and present methods to reduce the quantum resources required in its quantum circuit construction, measured in R_z gate counts and depths (see Sec. III).

In the case where we consider a quantum-classical hybrid approach more suitable for the pre-FT regime, we consider the widely-adopted technique of the variational quantum eigensolver [11]. Specifically, we aim to implement $U_{\text{ansatz}} = e^{(T-T^\dagger)}$ on a quantum computer, where T is the cluster operator, defined according to the unitary coupled cluster (UCC) approach [21, 22]. By tuning the variational parameters in T , in a typical VQE approach, $\langle \psi_0 | U_{\text{ansatz}}^\dagger H U_{\text{ansatz}} | \psi_0 \rangle$ is minimized, where $|\psi_0\rangle$ is an initial state that is assumed to be close to the target ground state of H and can readily be prepared on a quantum computer. The goal of this hybrid approach is then to estimate the ground state energy of the fermionic system with the Hamiltonian of the form (1). We show in this paper a complementary approach, based on the perturbation theory, to the hybrid method described above in order to better and more efficiently estimate the ground state energy (see Sec. IV A). Our perturbative approach induces a negligible quantum resource overhead, measured in the number of multi-qubit gates. We also consider different fermion to qubit transformations other than the aforementioned JW transformation (see Sec. IV B), which help reduce the number of multi-qubit gates without any loss in the algorithmic accuracy.

III. FAULT-TOLERANT REGIME - TIME EVOLUTION SIMULATION

As discussed in Section II, in this section, we detail the methods to optimize the time-evolution operator implementation on a quantum computer. In particular, we consider the PF approach. The cost function we consider are the number of R_z gates and the R_z gate depth, expected to be good proxy measures for the FT-regime quantum resource requirements.

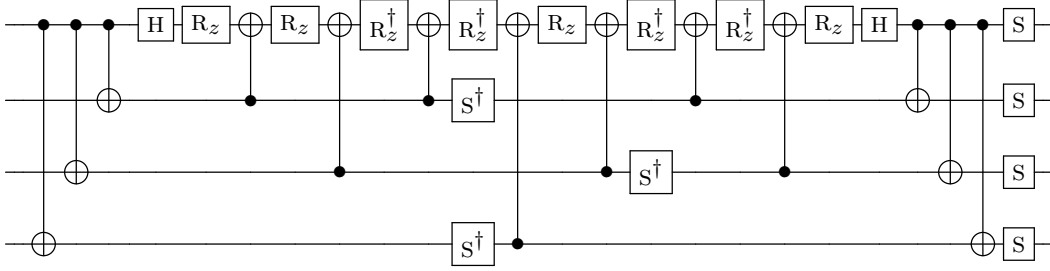


FIG. 1. Standard two-body interaction circuit that implements $\exp[-i(\theta/2)\sigma_+ \otimes \sigma_+ \otimes \sigma_- \otimes \sigma_- + \text{h.c.}]$. Following the steps detailed in [4] closely, expanding $\sigma_+\sigma_+\sigma_-\sigma_- + \text{h.c.}$ (we suppressed \otimes hereafter whenever contextually clear) into the particular ordering of $\sigma_x\sigma_x\sigma_x\sigma_x$, $\sigma_x\sigma_x\sigma_y\sigma_y$, $\sigma_x\sigma_y\sigma_y\sigma_x$, $\sigma_x\sigma_y\sigma_x\sigma_y$, $\sigma_y\sigma_y\sigma_x\sigma_x$, $\sigma_y\sigma_x\sigma_x\sigma_y$, $\sigma_y\sigma_x\sigma_y\sigma_x$, $\sigma_y\sigma_y\sigma_y\sigma_y$, and implementing them one after the other with last qubit as the target qubit, the circuit shown in this figure may be obtained after applying the circuit optimization routines detailed in [4, 24].

For completeness, we start by introducing the $2k^{\text{th}}$ order PF algorithm, simulating the fermionic system described in Section II. Assuming the JW transformation has been performed on the Hamiltonian H in (1), the time evolution operator we aim to implement may be written as

$$\exp\left(-i \sum_{j=1}^L \theta_j \hat{\sigma}^{(j)}\right) \approx [S_{2k}(\lambda)]^r, \quad (4)$$

where $\lambda := 1/r$, $\hat{\sigma}^{(j)} = \bigotimes_i \tilde{\sigma}^{(i,j)} + \text{h.c.}$, where $\tilde{\sigma}^{(i,j)} \in \{\sigma_+, \sigma_-, \sigma_z\}$, h.c. denotes the Hermitian conjugate operator, and

$$\begin{aligned} S_1(\lambda) &:= \prod_{j=1}^L \exp(-i\theta_j \hat{\sigma}^{(j)} \lambda), \\ S_2(\lambda) &:= \prod_{j=1}^L \exp(-i\theta_j \hat{\sigma}^{(j)} \lambda/2) \prod_{j=L}^1 \exp(-i\theta_j \hat{\sigma}^{(j)} \lambda/2), \\ S_{2k}(\lambda) &:= [S_{2k-2}(p_k \lambda)]^2 S_{2k-2}((1 - 4p_k)\lambda) [S_{2k-2}(p_k \lambda)]^2, \end{aligned} \quad (5)$$

with $p_k := 1/(4 - 4^{1/(2k-1)})$ for $k > 1$ [23]. Inspecting (5), together with (4), we observe that the individual exponential terms, hereafter referred to as a Trotter term, are of the form $\exp[-i\theta'_j(\bigotimes_i \tilde{\sigma}^{(i,j)} + \text{h.c.})]$, where θ'_j is a suitably scaled θ_j . A standard circuit that implements a Trotter term is readily available in [13]. Employing the circuit tricks in [4], in Fig. 1, we show an optimized quantum circuit that implements an exemplary Trotter term $e^{-i\theta/2(\sigma_+\sigma_+\sigma_-\sigma_- + \text{h.c.})}$.

To more efficiently implement the two-body term in the R_z counts, we first directly evaluate the operator. It is straightforward to see that the two-body term $e^{-i\theta/2(\sigma_+\sigma_+\sigma_-\sigma_- + \text{h.c.})}$ implements a R_x -rotation between $|0011\rangle$ state and $|1100\rangle$ state. Note that, for an input state of $|b_0 b_1 b_2 b_3\rangle$, where the m^{th} qubit variable b_m are either 0 or 1, $|b_0 \ b_1 \oplus b_2 \ b_0 \oplus b_2 \ b_0 \oplus b_3\rangle$ maps $|0011\rangle$ to $|0111\rangle$ and $|1100\rangle$ to $|1111\rangle$. A triply controlled R_x rotation on the zeroth qubit would thus implement the desired rotation on the mapped state, and all that needs

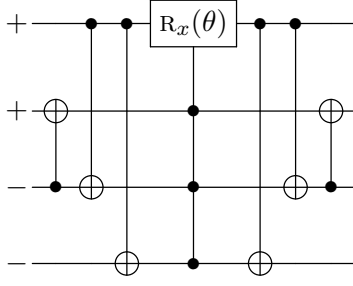


FIG. 2. FT-regime optimized circuit for the two-body term $e^{-i\theta/2(\sigma_+\sigma_+\sigma_-\sigma_-+\text{h.c.})}$. We marked each qubit lines with either + or - to denote which qubits are associated with σ_+ or σ_- , respectively, for this particular example.

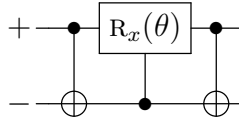
to be done at this point is to map the rotated state back. We show a quantum circuit that implements the two-body term, constructed according to aforementioned method, in Fig. 2.

A triply-controlled R_x gate in Fig. 2 may be implemented using single- and two- qubit gates. Specifically, we chose to use relative-phase triply controlled NOT gates (see [25] for its decomposition into single- and two- qubits gates), as shown in Fig. 3(a). We note that the circuit shown in Fig. 3(a) decreases the R_z count per two-body Trotter term from the standard eight to two.

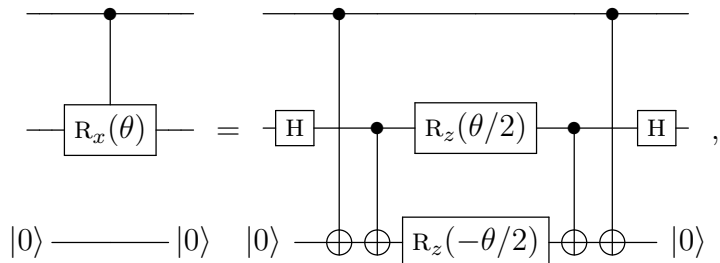
To further optimize the circuit for R_z -gate depth, we propose the following. Introducing a $|0\rangle$ -state initialized ancilla qubit, we can implement the same Trotter term as shown in Fig. 3(b). The circuit shown in Fig. 3(b) requires R_z depth of one per two-body Trotter term. Thus, this construction is likely R_z -depth optimal for a two-body Trotter term implementation, useful for the FT regime Fermion simulations.

If there are $\sigma_{x,y,z}$ operators that act on some other qubits, e.g., due to the JW transformation, we may simply modify the two-body circuit as follows. Consider, for example, there is a σ_z operator acting on an additional qubit. In this case, to implement $e^{-i\theta/2(\sigma_+\sigma_+\sigma_-\sigma_-\sigma_z+\text{h.c.})}$, we can modify the circuit in Fig. 2 and obtain the circuit shown in Fig. 4.

We next briefly describe a way to optimize the R_z depth of the single-body term. For the single-body operator $e^{-i\theta/2(\sigma_+\sigma_-+\text{h.c.})}$, in analogy to the two-body case shown above, we may use



to implement the operator. To now implement the controlled R_x gates optimally in terms of R_z -gate depth, we implement the gate by



which, inserted to the single-body operator circuit, results in a R_z depth one circuit.

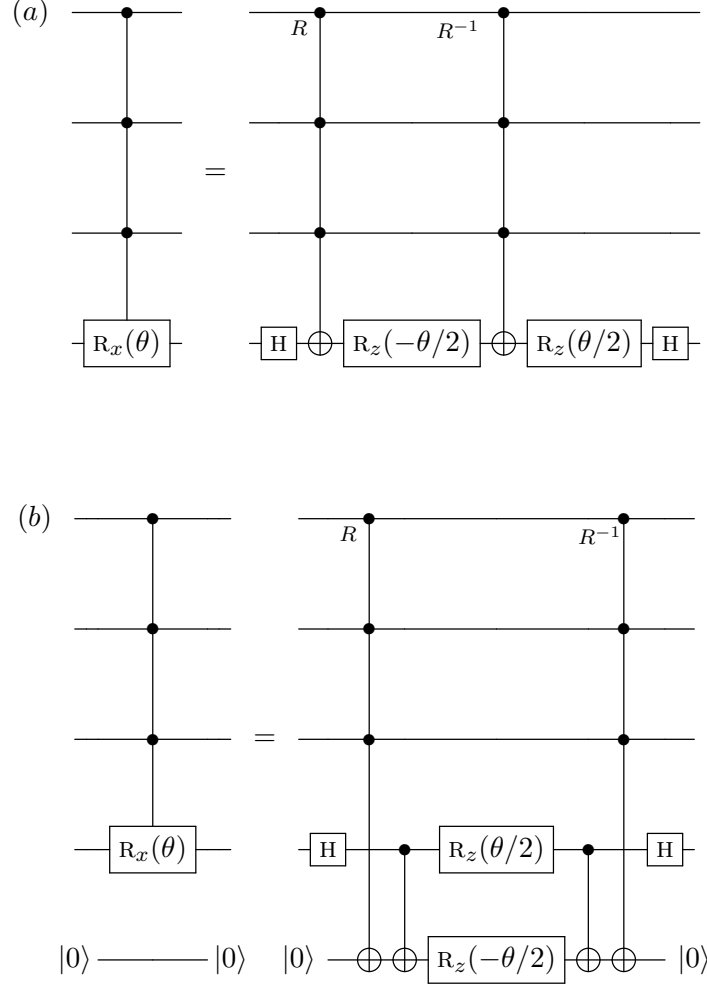


FIG. 3. Triply-controlled $R_x(\theta)$ gate implementation with relative-phase triply-controlled NOT gates. The R -prepended triply-controlled Toffoli gate denotes a relative-phase Toffoli gate, i.e., the gate implements a triply-controlled-NOT gate up to relative phases. The R^{-1} -prependix is used to denote its inverse. The method to implement the relative-phase Toffoli gate is detailed in [25–27].

IV. PRE-FAULT TOLERANT REGIME - VARIATIONAL QUANTUM EIGENSOLVER

In the pre-FT regime, we aim to calculate the ground state energy of the system whose Hamiltonian is given in the form (1). This is typically achieved by the VQE approach. In this approach, by iteratively calling the quantum computer to compute the energy of parametrized ansatz states, one aims to minimize the energy and variationally obtain the ground state of the target system.

Specifically, we consider a widely-adopted UCC ansatz, a systematic method that is universally applicable to any quantum hardware backend. We consider the case where the approach starts with energy and wavefunction obtained from the classically easily applicable Hartree-Fock (HF) method. The UCC method then evolves the ground state HF wavefunction $|\Psi_0\rangle$ with a unitary operator $U = e^{T-T^\dagger}$, where $T = \sum_l T_l$ is the cluster operator and

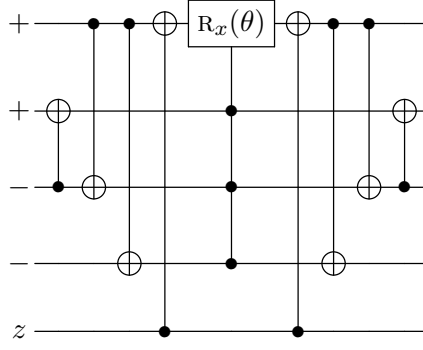


FIG. 4. FT-regime optimized circuit for the two-body term $e^{-i\theta/2(\sigma_+\sigma_+\sigma_-\sigma_-\sigma_z+\text{h.c.})}$. We marked each qubit lines with +, -, or z to denote which qubits are associated with σ_+ , σ_- , or σ_z , respectively, for this particular example.

T_l are the l -fold excitation operators. For instance, in second quantization,

$$\begin{aligned}
 T_1 &= \sum_{\substack{p \in \text{virt} \\ q \in \text{occ}}} t_{pq} a_p^\dagger a_q, \\
 T_2 &= \sum_{\substack{p, q \in \text{virt} \\ r, s \in \text{occ}}} t_{pqrs} a_p^\dagger a_q^\dagger a_r a_s,
 \end{aligned} \tag{6}$$

where t_{pq} and t_{pqrs} are variational parameters and “virt” and “occ” denote virtual and occupied levels respectively. A pre-FT quantum computer is then used to evolve the initially prepared Hartree-Fock ground state to ansatz states, while the coefficients in the cluster operator, t_{pq} and t_{pqrs} , are varied to minimize the energy $\langle \Psi_0 | U^\dagger H U | \Psi_0 \rangle$. Since a suitably transformed Hamiltonian H is of the form $H = \sum_j h_j \hat{\sigma}^{(j)}$, the energy expectation value maybe written as

$$\begin{aligned}
 \langle \Psi_0 | U^\dagger H U | \Psi_0 \rangle &= \sum_j h_j \langle \Psi_0 | U^\dagger \left[\bigotimes_i \hat{\sigma}^{(i,j)} \right] U | \Psi_0 \rangle \\
 &= \sum_j h_j \left(\sum_p \left| \langle \psi_j^{(p)} | U | \Psi_0 \rangle \right|^2 - \sum_m \left| \langle \psi_j^{(m)} | U | \Psi_0 \rangle \right|^2 \right),
 \end{aligned} \tag{7}$$

where $|\psi_j^{(p)}\rangle$ and $|\psi_j^{(m)}\rangle$ are the eigenvectors of $\hat{\sigma}^{(j)}$ with eigenvalues +1 and -1, respectively. Therefore, the energy expectation value can be evaluated efficiently on a quantum computer, where the quantum resource cost of this hybrid approach is the implementation cost of the operator U .

In this section, we discuss two general procedures to reduce circuit complexity of the approach detailed above, represented by the total number of multi-qubit gates. To be concrete, we use the first-order PF algorithm to implement the UCC ansatz, although extensions to any higher order PF algorithms are straightforward. In Sec. IV A, we detail a hybrid framework that is based on the perturbation theory, wherein we apply perturbation correction to each instance of the VQE circuit and determine the important ansatz terms to include in the larger instance of the VQE circuit based on the correction in the smaller instance of

the VQE circuit, effectively bootstrapping the VQE progression towards the ground-state energy estimate of the simulated system. In Sec. IV B, we explore a suite of generalized fermion to qubit operator transformations to reduce the cost of quantum computation without sacrificing algorithmic accuracy.

A. Perturbation Assisted Quantum Simulation

In this section, we describe a general framework that leverages the power of perturbation theory to optimize VQE-based quantum simulations by predicting the ansatz terms to include in the UCC ansatz and correcting the VQE result via post processing. The framework optimizes both the total number of VQE executions as well as the size of the ansatz state preparation circuits used to reach the convergence in the ground-state energy estimate. In Sec. IV A 1 we outline the framework. The derivation of a simple perturbation scheme that can be straightforwardly implemented in the framework is shown in Sec. IV A 2, which we hereafter refer to as a hybrid second order Møller-Plesset perturbation (HMP2) method. In Sec. IV A 3 we present a classically simulated comparison between the HMP2 scheme and a more conventional VQE approach [4], by computing the ground state energy of a water molecule.

1. Perturbative predictor and corrector

We detail, in this section, a general, systematic way of using perturbation methods to improve quantum resources required for the VQE approach. Specifically, we aim to rapidly converge to the ground state energy with small quantum circuits. A critical part in ensuring the rapid convergence is the selection of individual excitation terms in (6) used to prepare the ansatz state. Previous works have, e.g., used the full configuration interaction (FCI) results [4] in the case the system is sufficiently small to be simulatable on a classical computer, and have demonstrated the significance of the excitation term selection in the resource requirement. Here, we propose to iteratively select a next excitation term to consider in the ansatz state preparation based on the size of the perturbatively predicted amplitude for the excitation term for a given ansatz state whose variational parameters are already optimized via the conventional means of the VQE. Our strategy also evaluates perturbative energy correction in addition to the conventional VQE approach, directly contributing to the fast convergence, while incurring no overhead in the pre-FT regime resource requirement.

Figure 5 shows the flow diagram of the proposed framework. As in the conventional VQE approach for fermionic simulations, we start with a single particle Hamiltonian and its ground state wavefunction which has already been properly antisymmetrized. Using the two-particle Hamiltonian as perturbation, energy and wavefunction corrections can be calculated using classical algorithms with relative ease. From the perturbed wavefunction, we can extract the amplitudes of individual excited states in the single-particle Hamiltonian basis. These amplitudes will serve as the initial guesses of the variational parameters for the first round of VQE simulation, which could significantly reduce the number of evaluations of the quantum circuit comparing to all-zeros or random initial guesses [28]. If we demand the energy convergence criteria of δ_E – The entire simulation is considered to be converged when the magnitude of energy change associated with addition of any extra ansatz term is smaller than δ_E – we include in the initial ansatz set the ansatz terms whose contribution

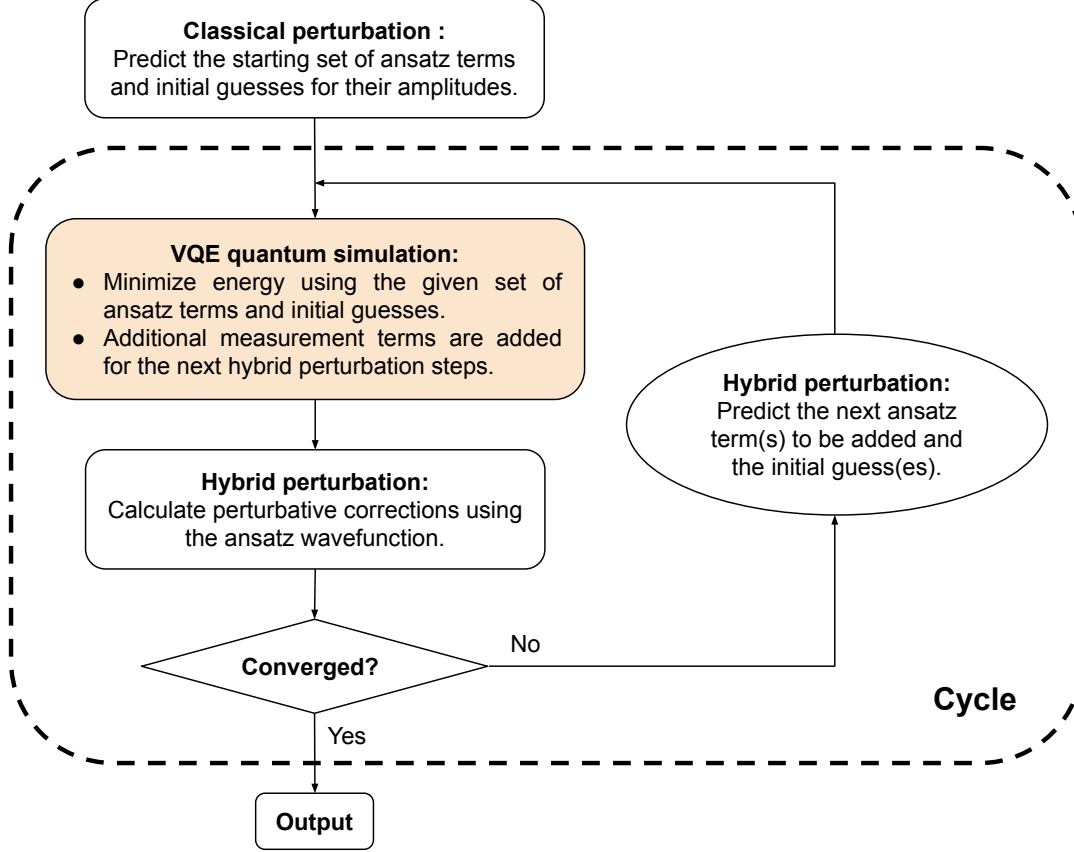


FIG. 5. Flow diagram for the proposed framework incorporating perturbation methods to VQE simulations. See main text for detailed description.

to correlation energy is greater than $f(\delta_E)$, where a standard choice of function $f(\delta_E)$ may simply be δ_E .

With the initial set of ansatz terms and their initial variational parameter values, we run the first round of VQE simulation to minimize the energy $\langle \Psi_{\text{ansatz}} | H | \Psi_{\text{ansatz}} \rangle$. Once the energy is minimized and the ansatz state converges, we proceed to compute the expectation values of a set of operators that were chosen in advance to inform us about the perturbation around the converged ansatz state. We refer to this method as a hybrid perturbation since unlike the conventional perturbation where we know the unperturbed wavefunction in advance, we start the perturbation from the converged VQE ansatz state.

Based on the additional measurements performed on a quantum computer, we may now use the hybrid perturbation method to calculate corrections to the correlation energy and approximate amplitudes for the ansatz terms to be added to the next cycle of the VQE. The resulting total energy of this cycle is the summation of the energy correction and the VQE energy. The ansatz term with the largest amplitude that results from the hybrid perturbation may for instance be added to the next cycle of the VQE simulation, with initial variational parameter being based on the approximate amplitude. The initial variational parameter values of the ansatz terms that continue to be a part of the next VQE simulation may simply be imported from the cycle before.

The cycle iterates the outlined procedure of running the VQE simulation and the hybrid

perturbation calculation, until the convergence of the total energy is achieved. We next detail the steps of our hybrid perturbation method.

2. HMP2 method

We derive in this section our hybrid perturbation method, inspired by the Møller-Plesset perturbation theory, applied to the VQE simulation using UCC ansatz. We use Z for the truncated cluster operator in the UCC operator $U = e^{Z-Z^\dagger}$. Our hybrid MP2-based perturbation method, HMP2, then aims to accurately estimate the lowest eigenvalue of H . Since U is unitary, this is equivalent to obtaining the lowest eigenvalue of $U^\dagger H U$. We can thus write the UCC energy E_{UCC} in the context of the first-order perturbation theory, i.e.,

$$\begin{aligned}
E_{UCC} &= \langle \Psi_0 | U^\dagger H U | \Psi_0 \rangle \\
&= \langle \Psi_0 | F + (U^\dagger H U - F) | \Psi_0 \rangle \\
&= \langle \Psi_0 | F | \Psi_0 \rangle + \langle \Psi_0 | U^\dagger H U - F | \Psi_0 \rangle \\
&= E_0 + (E_{UCC} - E_0) \\
&= E^{(0)} + E^{(1)},
\end{aligned} \tag{8}$$

where F is the Fock operator, E_0 is the sum of orbital energies, $E^{(0)} = E_0$ is the zeroth-order correction energy, and $E^{(1)} = E_{UCC} - E_0$ is the first-order correction energy. Based on the standard perturbation theory, the second order correction to the energy can now be written as

$$E^{(2)} = \sum_{D_{\{\alpha\}}} \frac{\left| \langle \Psi_{D_{\{\alpha\}}} | V | \Psi_0 \rangle \right|^2}{\Delta E_{D_{\{\alpha\}}}}, \tag{9}$$

where $V = U^\dagger H U - F$, $D_{\{\alpha\}}$, which substitute the orbitals in a wavefunction according to the set of orbital sequence $\{\alpha\}$, is a generic orbital substitution operator. For instance, a single orbital substitution operator $D_{pq} = a_p^\dagger a_q$ substitute orbital q with p . Then we can define the substituted wavefunction $|\Psi_{D_{\{\alpha\}}}\rangle = D_{\{\alpha\}} |\Psi_0\rangle$. The energy $\Delta E_{D_{\{\alpha\}}}$ is defined as the orbital energy difference of the orbital substitution. For instance, $\Delta E_{D_{pq}} = \epsilon_q - \epsilon_p$, where ϵ_p and ϵ_q are the orbital energies of p^{th} and q^{th} orbitals, respectively. Inserting $V = U^\dagger H U - F$ in (9), the numerator of (9) becomes

$$\begin{aligned}
\left| \langle \Psi_{D_{\{\alpha\}}} | V | \Psi_0 \rangle \right|^2 &= \left| \langle \Psi_{D_{\{\alpha\}}} | U^\dagger H U - F | \Psi_0 \rangle \right|^2 \\
&= \left| \langle \Psi_{D_{\{\alpha\}}} | U^\dagger H U | \Psi_0 \rangle - \langle \Psi_{D_{\{\alpha\}}} | F | \Psi_0 \rangle \right|^2 \\
&= \left| \langle \Psi_{D_{\{\alpha\}}} | U^\dagger H U | \Psi_0 \rangle \right|^2,
\end{aligned} \tag{10}$$

where we used $\langle \Psi_{D_{\{\alpha\}}} | F | \Psi_0 \rangle = 0$.

In order to apply the UCC results directly to the perturbation calculation, we proceed as follows. First, for brevity, we drop $\{\alpha\}$ wherever contextually clear. We also introduce

$\tilde{Z} = Z - Z^\dagger$ so that $U = e^{\tilde{Z}}$. We further introduce $\tilde{D} = D - D^\dagger$. Inserting these into (10), we obtain

$$\begin{aligned} |\langle \Psi_D | U^\dagger H U | \Psi_0 \rangle|^2 &= |\langle \Psi_0 | \tilde{D}^\dagger U^\dagger H U | \Psi_0 \rangle|^2 \\ &= |\langle \Psi_{UCC} | U \tilde{D}^\dagger U^\dagger H | \Psi_{UCC} \rangle|^2 \\ &= |\langle \Psi_{UCC} | e^{\tilde{Z}} \tilde{D}^\dagger e^{-\tilde{Z}} H | \Psi_{UCC} \rangle|^2. \end{aligned} \quad (11)$$

Next we Taylor expand the $e^{\pm\tilde{Z}}$ in $e^{\tilde{Z}} \tilde{D}^\dagger e^{-\tilde{Z}} H$ up to first order in \tilde{Z} . We obtain

$$\begin{aligned} |\langle \Psi_{UCC} | e^{\tilde{Z}} \tilde{D}^\dagger e^{-\tilde{Z}} H | \Psi_{UCC} \rangle|^2 &= |\langle \Psi_{UCC} | (1 + \tilde{Z} + \dots) \tilde{D}^\dagger (1 - \tilde{Z} + \dots) H | \Psi_{UCC} \rangle|^2 \\ &\approx |\langle \Psi_{UCC} | \tilde{D}^\dagger H - \tilde{D}^\dagger \tilde{Z} H + \tilde{Z} \tilde{D}^\dagger H | \Psi_{UCC} \rangle|^2. \end{aligned} \quad (12)$$

We note that $\tilde{D}^\dagger H - \tilde{D}^\dagger \tilde{Z} H + \tilde{Z} \tilde{D}^\dagger H$ is a sum of products of Pauli operators $\sum_j \epsilon_j \hat{\sigma}^{(j)}$ in the qubit basis, after applying a suitable fermion to qubit basis transformation. Since $\hat{\sigma}^{(j)}$ have eigenvalues $+1$ or -1 , we may then write

$$\begin{aligned} \left| \left\langle \Psi_{UCC} \left| \sum_j \epsilon_j \hat{\sigma}^{(j)} \right| \Psi_{UCC} \right\rangle \right|^2 &= \left| \left\langle \Psi_{UCC} \left| \sum_j \epsilon_j \left(\sum_p |\psi_j^{(p)}\rangle \langle \psi_j^{(p)}| - \sum_m |\psi_j^{(m)}\rangle \langle \psi_j^{(m)}| \right) \right| \Psi_{UCC} \right\rangle \right|^2 \\ &= \left| \sum_j \epsilon_j \left(\sum_p |\langle \Psi_{UCC} | \Psi_j^{(p)} \rangle|^2 - \sum_m |\langle \Psi_{UCC} | \Psi_j^{(m)} \rangle|^2 \right) \right|^2. \end{aligned} \quad (13)$$

Note that (13) requires only a simple projection of $|\Psi_{UCC}\rangle$ onto $\Psi_j^{(p)}$ or $\Psi_j^{(m)}$. Thus the second order correction energy maybe obtained without any resource overhead in the circuit size.

The first order wavefunction correction is given by

$$|\Psi_{\text{correction}}^{(1)}\rangle = \sum_D \frac{\langle \Psi_D | V | \Psi_0 \rangle}{\Delta E_D} |\Psi_D\rangle. \quad (14)$$

The amplitudes of the ansatz terms not present in Z can then be approximated as $\langle \Psi_D | V | \Psi_0 \rangle / \Delta E_D$. We use these amplitudes to determine the next ansatz term to include in our UCC ansatz, if the ground-state energy estimates has not been converged.

We note in passing that, in principle, the number of individual operators whose expectation values are to be evaluated using a quantum computer scales as $O(n^8)$ per UCC ansatz where n is the number of qubits. While this may appear challenging, in practice, a series of techniques can be applied to significantly reduce the number of evaluations. See Supplementary Material (SM) Sec. S7 for detail. Fig. 6 shows an example case for the water molecule for the number of Pauli strings that need to be measured in a quantum computer before and after the optimization. Compared to the pre-optimization number of measurements, the optimized number of Pauli strings that need to be measured is more than two orders of magnitude smaller.

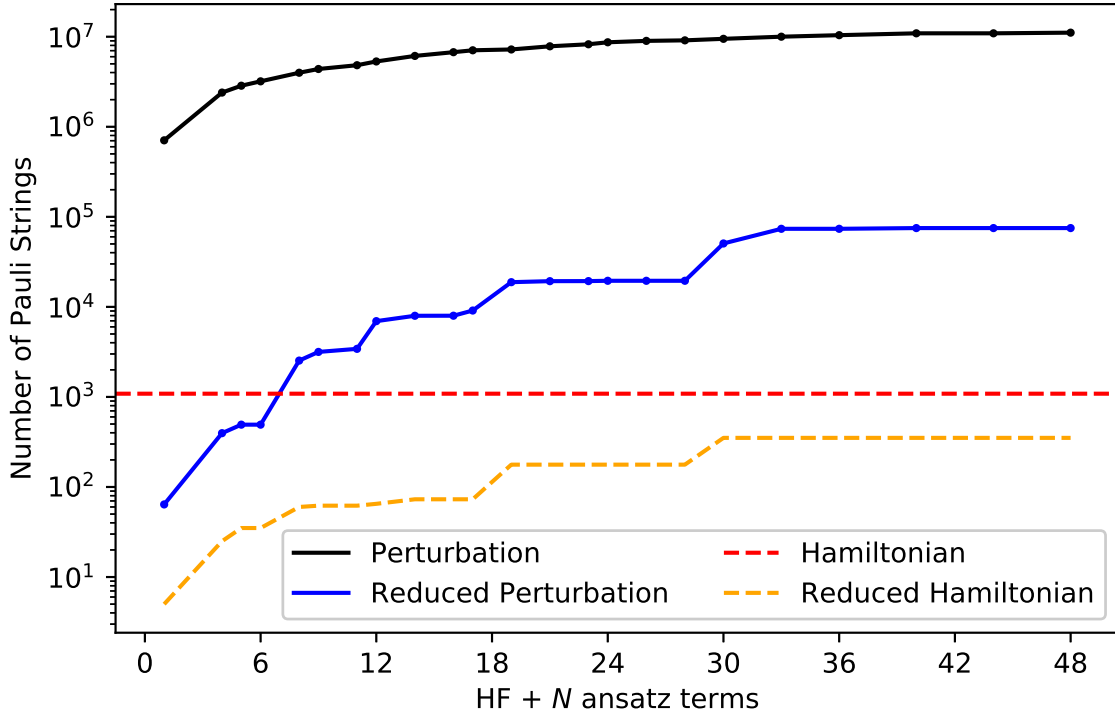


FIG. 6. Number of Pauli strings that need to be measured before and after the optimization for an exemplary case of a water molecule with STO-3G basis. The order in which we add the ansatz terms is found according to the HMP2 method. For completeness, we also show the number of Pauli strings that stem from the Hamiltonian.

3. Comparison to prior state-of-the-art

To demonstrate our framework of perturbation assisted quantum simulation using the HMP2 method, we perform classically emulated VQE calculations of the ground state energy of a water molecule at its equilibrium geometry. Using STO-3G basis, the calculation contains 14 qubits in total. Table I shows the incremental changes of UCC correlation energy as well as HMP2 correction as more ansatz terms are included according to our framework. To compare, we also listed the classically calculated HF, MP2, CCSD, and FCI energies. With the HMP2 correction, the total energy $E_{\text{UCC+HMP2}}$ descends quickly towards FCI energy.

Figure 7 shows the convergence of the ground state energies using different approaches as the number of terms N included in the UCC operator increases. For the conventional approach [4], the insertion order of the ansatz terms is obtained from the prior knowledge of the order of contribution of determinants in a classical FCI calculation, which closely mimics the ideal case but rarely realistic to obtain. For the UCC energies obtained using the proposed HMP2, we bootstrapped the ordering of the ansatz terms as detailed in Sec. IV A 2. Comparing the convergence of the UCC energies, we find that the HMP2-bootstrapped ordering effectively captures the major ansatz terms. This is confirmed by the good agreement between the FCI ordering and the HMP2 ordering shown in Fig. 7. We also observe that the HMP2 correction to the ground-state energy helps accelerate the energy convergence to-

Ansatz	E_{UCC}	$E_{\text{PD}}^{\text{corr}}$	$E_{\text{UCC+HMP2}}$	
Ansatz terms in HMP2 order	HF+1	-74.9749	-0.0249	-74.9998
	HF+2	-74.9781	-0.0220	-75.0001
	HF+4	-74.9854	-0.0170	-75.0024
	HF+5	-74.9881	-0.0155	-75.0036
	HF+6	-74.9909	-0.0139	-75.0048
	HF+8	-74.9966	-0.0091	-75.0057
	HF+9	-74.9996	-0.0068	-75.0063
	HF+11	-75.0038	-0.0039	-75.0077
	HF+12	-75.0047	-0.0034	-75.0081
	HF+14	-75.0074	-0.0023	-75.0098
	HF+16	-75.0091	-0.0015	-75.0106
	HF+17	-75.0100	-0.0009	-75.0109
	HF+19	-75.0102	-0.0007	-75.0109
	HF+21	-75.0107	-0.0004	-75.0111
	HF+23	-75.0111	-0.0002	-75.0113
	HF+24	-75.0113	-0.0001	-75.0114
	HF+26	-75.0113	-0.0001	-75.0114
	HF+28	-75.0113	-0.0001	-75.0114
<hr/>				
E_{HF}			-74.9624	
E_{MP2}			-74.9977	
E_{CCSD}			-75.0114	
E_{FCI}			-75.0116	

TABLE I. Ground state energy calculations for a water molecule using STO-3G basis. HF+ N represents a VQE cycle with UCC ansatz with N terms, as described in Sec. IV A 1. $E_{\text{P}_D}^{\text{corr}}$ is the HMP2 correction based on (12). $E_{\text{UCC+HMP2}} = E_{\text{UCC}} + E_{\text{P}_D}^{\text{corr}}$ is the total energy obtained in one VQE cycle. The classically computed energies E_{HF} , E_{MP2} , E_{CCSD} , and E_{FCI} for the water molecule with the same geometry and basis set are also listed for comparison. All energies are in units of Hartree.

wards the FCI energy significantly. Provided that implementation of each additional ansatz term leads to a substantial accumulation of noise in the NISQ hardware, we find the rapid energy convergence enabled by the HMP2 method to be particularly useful for the near-term quantum computers.

B. Generalized transformations for Fermion to Qubit operator

In this section, we investigate how a variety of fermion to qubit transformations may be used to reduce the quantum resource requirements for the pre-FT fermion simulations. It is important to note that all of the transformations are equivalent and thus the resulting quantum circuits for each transformations implement exactly the same fermion simulation. Therefore, the resource savings we obtain in this section are independent of the accuracy of the simulations, in general.

Well-known fermion to qubit transformations, such as the Jordan-Wigner (JW) [15] or Bravyi-Kitaev (BK) [16] transformations, map fermionic creation (annihilation) operators

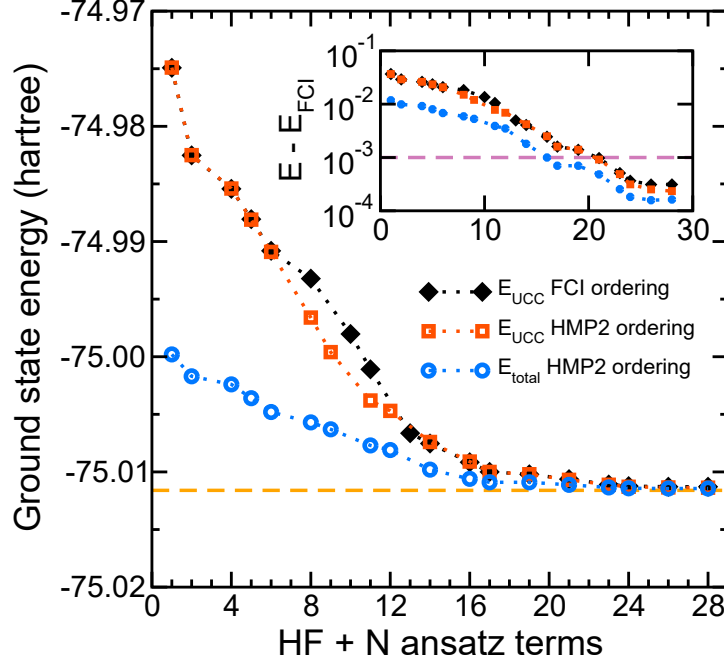


FIG. 7. Comparison of the ground state energies of a water molecule at its equilibrium geometry using STO-3G basis set, calculated by various methods as a function of N , the number of ansatz terms included. The orange dashed line is the FCI energy calculated using PSI4 package [29], which serves as the benchmark. The black filled diamonds connected by dotted lines are the UCC energies E_{UCC} , calculated using different number of ansatz terms ordered by the contribution of corresponding determinants to the FCI energy. The open squares and open circles connected by dotted lines are the ground-state energies computed according to the proposed framework with the HMP2 ordering, with the open circles containing the additional HMP2 energy correction at each VQE cycle. The inset shows in semi-log the differences between the energies obtained by the aforementioned methods and the FCI energy as a function of N . The purple dashed line shows the chemical accuracy given by 10^{-3} hartree.

to Pauli strings. However, there in principle exist numerous other transformations available for use. Below, we introduce a generalized transformation (GT) method (see also [17]), of which the JW and BK transformations are a part. We show that, when used with the PF algorithm as a concrete example for the implementation of the UCC ansatz, significant quantum resource savings may be achieved by a suitable choice of the mapping for a given cluster operator input, together with a carefully chosen sequence of heuristic optimization methods.

All transformations in the GT method must respect relations specified in (2). This may be achieved by considering the following invertible, upper-triangular basis-transformation matrix β , which transforms the occupation number basis to a GT basis according to

$$\beta = \begin{pmatrix} \beta_{n-1,n-1} & \beta_{n-1,n-2} & \dots & \beta_{n-1,0} \\ 0 & \beta_{n-2,n-2} & \dots & \beta_{n-2,0} \\ \vdots & \vdots & & \vdots \\ 0 & 0 & \dots & \beta_{0,0} \end{pmatrix}, \quad (15)$$

where $\beta_{i,j} \in \{0, 1\}$ and n is the number of qubits. Following closely the notations used in [30], we define the following sets of indices for convenience, which we detail below. We note that all matrix operations are performed in modulo-2 space and the main diagonal elements are excluded when generating these sets.

- Update set $U(j)$: elements of this set are the row indices with non-zero entries in column j of the basis-transformation matrix β .
- Parity set $P(j)$: elements of this set are the column indices with non-zero entries in row j of the matrix $(\pi\beta^{-1} - \beta^{-1})$, where $\pi_{i,j} = 1$ if $i \leq j$, otherwise 0.
- Remainder set $R(j)$: elements of this set are the column indices with non-zero entries in row j of the matrix $\pi\beta^{-1}$.

The GT-based creation and annihilation operators are then

$$\begin{aligned} a_j^\dagger &\equiv [\sigma_x^{U(j)} \otimes \sigma_x^j \otimes \sigma_z^{P(j)} - i\sigma_x^{U(j)} \otimes \sigma_y^j \otimes \sigma_z^{R(j)}] / 2, \\ a_j &\equiv [\sigma_x^{U(j)} \otimes \sigma_x^j \otimes \sigma_z^{P(j)} + i\sigma_x^{U(j)} \otimes \sigma_y^j \otimes \sigma_z^{R(j)}] / 2, \end{aligned} \quad (16)$$

which can straightforwardly be shown to satisfy (2). We note that, e.g., the JW transformation is a special case of $\beta = \mathbf{1}$.

Previous state of the art [4] in the resource requirement for the UCC ansatz implementation relies on the JW transformation and it considers a series of heuristics that were chosen carefully to optimize the resulting quantum circuits. To enable a proper comparison of those with our results then, it is necessary for us to consider a similar series of heuristics as well. Details of the heuristics we consider are provided in the SM Secs. S1–S6. Below, we briefly outline the steps in the order of applications. The cost function we considered for our concrete example is the number of two-qubit gates.

The outer-most loop of our approach considers different transformation matrices β . For a given mapping matrix β , we execute the following routines to construct and optimize our circuit that implements the UCC ansatz. The routines are designed to repeatedly call a suite of dedicated, automated circuit optimization tools, whose technical details may be found in [4, 24]. The efficiency of these tools allows us to quickly evaluate the cost function for different cases we consider in each of the subroutines.

Routine 1 *Fermionic level labeling*: Unlike in the JW transformation where $U(j)$ is an empty set and $P(j) = R(j)$, in the GT approach, myriads of combinations of sets $U(j)$, $P(j)$, and $R(j)$ are possible. To best take advantage of this, it is critical to carefully select which fermion level is mapped onto which qubit index. Exploring all possible mapping is however computationally prohibitively expensive. We thus resort to a simple greedy approach, whereby we explore one permutation at a time from a given fermion-level to qubit-index mapping. Specifically, from the given mapping, we apply the permutation that results in the most reduction in the quantum resource requirements. We iterate this process until no single permutation results in the reduction of quantum resource requirements. See SM Sec. S1 for detail. See **Subroutine 1** below for the cost function evaluation for each permutation.

Routine 2 *Inter-Trotter term ordering:* Demonstrated in [4] was that ordering the Trotter terms appropriately can lead to large savings in the two-qubit gate counts due to gate cancellations between the neighboring Trotter term circuits. While a similar approach is indeed possible, in our GT approach, a non-trivial modification needs to be made. Specifically, we need to preprocess each Trotter terms to determine their eligibility for being classified under the same equivalence class, the elements of which have the opportunities for resource savings when placed next to one another on a quantum circuit via the aforementioned gate cancellations. The eligibility criteria are straightforward for the JW transformation, considered in [4]. See SM Sec. S3 for details for the GT method. Once the equivalence classes according to the eligibility of each Trotter terms are determined, we use a simple greedy approach to order the Trotter-term elements of each equivalence classes to reduce the two-qubit gate counts.

Subroutine 1 *Intra-Trotter term ordering:* For a given fermion-label to qubit-index mapping, an efficient method to implement a single- or a two-fermion excitation Trotter term is known [4] in the case where the JW transformation is used. The method relies on a careful ordering of the intra-Trotter operator implementation, where, for instance, an exemplary two-fermion Trotter term $e^{t_{pqrs}(a_p^\dagger a_q^\dagger a_r a_s - h.c.)}$ is expanded to $\sigma_{x,y,z}$ -based intra-Trotter terms. To enable an efficient implementation in other transformations used in our GT approach, we compute the cost function for every possible permutations of the intra-Trotter terms (see SM Sec. S2 for detail). We choose an ordering with the least cost.

The resulting optimized circuit implements the UCC ansatz in the chosen transformation basis defined by β . However, with the exception of the JW transformation where $\beta = \mathbf{1}$, the GT β matrix requires us to implement the initial mapping of the basis at the beginning of the circuit. This incurs an overhead $O(n^2/\log(n))$ in the two-qubit gate counts [31], where n is the number of qubits. To obtain the final quantum resource requirement, we call the automated optimizer with the input quantum circuit that consists of the prefix subcircuit that implements β and the postfix subcircuit that implements β -basis UCC ansatz.

We note that in [4] the concept of “bosonic” excitations is discussed. Effectively, in the JW transformation, whenever a pair of neighboring qubits, whichever appropriate fermion levels they correspond to, are excited to yet another pair of neighboring qubits that denote another set of fermion levels, the circuit that implements such an excitation term can be dramatically simplified to require only two two-qubit gates, while requiring only half the number of qubits that would otherwise be required (see SM Sec. S4 for the cases where the pairs do not neighbor). To take advantage of this, we use a juxtaposition the bosonic circuit written according to the JW transformation and non-bosonic circuit written according to our GT approach. We note in passing that, to return from the half-qubit space of the bosonic circuit to the full-qubit space of the non-bosonic circuit, $n/2$ CNOT gates must be expended. All our circuit metrics appropriately reflect this.

Table II shows circuit metrics, measured according to the number of two-qubit gates used to implement a UCC ansatz circuit, for different molecules of our choice. We show the results for the JW, BK, and the best GT transformations that our heuristic toolchain specified above found for comparison. To find the best GT transformations, we used a

Molecule	NQ	NDE	JW	BK	GM	Improve(%)
HF	12	4	131	146	112	14.50
F ₂	20	6	236	238	189	19.92
N ₂	20	45	847	989	788	6.97
CO	20	56	961	116	918	4.47
LiH	12	8	204	207	177	13.66
BeH ₂	14	9	342	336	302	11.70
NH ₃	16	54	788	1048	787	0.13
<hr/>						
H ₂ O(8)	14	8	68	86	58	14.71
H ₂ O(10)	14	10	89	108	88	1.12
H ₂ O(11)	14	11	92	111	91	1.09
H ₂ O(13)	14	13	114	140	111	2.63
H ₂ O(14)	14	14	116	142	112	3.45
H ₂ O(16)	14	16	138	165	132	4.35
H ₂ O(17)	14	17	140	167	134	4.29
H ₂ O(19)	14	17	143	174	141	1.40
H ₂ O(21)	14	19	165	210	162	1.82

TABLE II. Number of two-qubit gates required for the VQE simulation of different molecules with different fermion to qubit transformations. NQ is the number of qubit required. NDE is the number of double excitation terms considered in the UCC ansatz. JW/BK are the number of two-qubit gates with JW or BK transformation β . GT is the number of two-qubit gates given by the best β other than JW or BK. All molecules use STO-3G basis. (Top): Considered in the UCC ansatz are all single excitation terms and the respective number of double excitation terms specified in the NDE-column, where we kept the most significant terms, ordered according to MP2 amplitudes. (Bottom): the parentheses next to H₂O indicate the total number of excitation terms considered for the UCC ansatz, selected according to the FCI contribution order.

particle swarm optimization, as detailed in SM Secs. S5 and S6. The advantages offered by the GT transformations vary in the suite of molecules we consider, ranging from 0.13% to 19.92%. This demonstrates the capability of our heuristics that it is indeed possible to further optimize the quantum circuits over the previous state of the art obtained via the JW transformation by considering GT transformations, custom selected for different input cases.

V. DISCUSSION

So far in this paper, in the optimization of the FT-regime circuits, we have considered efficient implementations of each Trotter terms. It should however be noted that a parallel implementation of multiple Trotter terms should also be considered in the R_z gate depth reduction of the quantum simulation circuits. Based on our circuit construction detailed in Sec. III, we propose the following methodology for optimization over the parallel implementation.

As discussed in Sec. III, note that the circuit that implements the Trotter term (see

Fig. 2) consists largely of three parts: an initial CNOT gate network that computes a linear function of Boolean input variables, a triply-controlled R_x gate, and the inverse of the initial CNOT gate network. Denoting the Boolean variables at the input as, in the order from top to bottom, a , b , c , and d , the CNOT gate network outputs a , $b \oplus c$, $a \oplus c$, $a \oplus d$. The bottom three outputs remain invariant over the action of the triply-controlled R_x gate. This means that any linear functions of $b \oplus c$, $a \oplus c$, $a \oplus d$ are accessible for use in the implementation of CNOT gates that correspond to the JW σ_z strings for other Trotter terms. This is so, because the invariance is required to implement the appropriate inverse of the CNOT gates that were used to take the JW σ_z strings into consideration in the first place, as per our circuit construction shown in Fig. 4. Heuristic methods that collect those Trotter terms that can simultaneously be implemented can then be used to optimize the depth of the quantum circuit.

For pre-FT regime VQE simulations, we have proposed a general framework that leverage the predictive and corrective power of perturbation theory. In addition to the HMP2 method described here, many more complex forms of perturbation theory can also be used to improve the efficiency and accuracy of the simulations. For instance, it is possible to obtain the coefficients for ansatz terms, possibly including triple or higher excitation terms perturbatively, similar to the way classical CCSD(T) or CCSDT-1a/b methods [32–34]. Our framework is general enough that these more complex perturbation methods can easily replace the HMP2 methods inside the simulation cycle.

We note that, extending and generalizing the framework used for considering the bosonic terms in the JW transformation and the non-bosonic terms in the GT transformation, the use of multiple fermion to qubit transformations β for a given set of excitation terms could be of value in reducing the overall resource requirement. Drawing from the fact that different β transformations result in different resource requirements in implementing the excitation terms of a target UCC ansatz circuit, it is reasonable to expect that a certain subset of the excitation terms may be more efficiently implemented by one β transformation and the rest of the excitation terms may be implemented more efficiently by yet another β transformation. Thus, dividing the set of excitation terms required for preparing a UCC ansatz state into subsets of excitation terms that may be more efficiently implemented by respective, appropriate choices of β transformations for each of the subset may prove to be more advantageous in the quantum resource requirement. Optimizing over the tug of war expected between the overhead cost incurred due to the switching of the transformations and the savings obtained via the tailor-made choices of the transformations remains as future work.

VI. CONCLUSION

Quantum simulations performed by quantum computers have long been thought to be one of the most promising quantum applications that will prove advantageous over classical computers. Despite the recent technological advancements made by the community, there still remains a gap between what a quantum device can realistically achieve and what is required to demonstrate a practical advantage in running a quantum simulation on a quantum device. In an attempt to bridge this gap, in this paper, we focused on optimizing the quantum resource requirements for both the FT and pre-FT regime quantum simulations of fermionic systems. Our approach yields a R_z -depth one quantum circuit for each Trotterized evolution operator, useful for the FT-regime quantum computers. We present the HMP2 framework,

bootstrapping the VQE method, to determine the best ansatz terms to consider next, in addition to those that are already considered in the original ansatz preparation circuit, by running the original ansatz preparation circuit itself on a pre-FT quantum computer. The HMP2 method provides an added benefit by improving the ground-state energy estimates via the second-order correction as well. We also considered GT methods to obtain significant quantum resource savings over the conventional JW or BK transformations in practice. While these results were applied to a specific set of fermionic systems in this paper as a concrete example, we expect similarly-spirited works could leverage our methodologies. We believe the savings in the quantum resource requirement demonstrated by our approaches help bring the day of solving practical problems using a quantum computer closer.

ACKNOWLEDGEMENT

This work was supported, in part, by the DOE BES QIS Program (de-sc0019449).

-
- [1] A. Kandala, A. Mezzacapo, K. Temme, M. Takita, M. Brink, J. M. Chow, and J. M. Gambetta, *Nature* **549**, 242 (2017).
 - [2] C. Hempel, C. Maier, J. Romero, J. McClean, T. Monz, H. Shen, P. Jurcevic, B. P. Lanyon, P. Love, R. Babbush, A. Aspuru-Guzik, R. Blatt, and C. F. Roos, *Physical Review X* **8**, 031022 (2018).
 - [3] P. J. J. O’Malley, R. Babbush, I. D. Kivlichan, J. Romero, J. R. McClean, R. Barends, J. Kelly, P. Roushan, A. Tranter, N. Ding, B. Campbell, Y. Chen, Z. Chen, B. Chiaro, A. Dunsworth, A. G. Fowler, E. Jeffrey, E. Lucero, A. Megrant, J. Y. Mutus, M. Neeley, C. Neill, C. Quintana, D. Sank, A. Vainsencher, J. Wenner, T. C. White, P. V. Coveney, P. J. Love, H. Neven, A. Aspuru-Guzik, and J. M. Martinis, *Physical Review X* **6**, 031007 (2016).
 - [4] Y. Nam, J.-S. Chen, N. C. Pienti, K. Wright, C. Delaney, D. Maslov, K. R. Brown, S. Allen, J. M. Amini, J. Apisdorf, A. Beck, Kristin M. Blinov, V. Chaplin, M. Chmielewski, C. Collins, S. Debnath, A. M. Ducore, K. M. Hudek, M. Keesan, S. M. Kreikemeier, J. Mizrahi, P. Solomon, M. Williams, J. D. Wong-Campos, C. Monroe, and J. Kim, *npj Quantum Information* **6**, 1 (2020).
 - [5] E. F. Dumitrescu, A. J. McCaskey, G. Hagen, G. R. Jansen, T. D. Morris, T. Papenbrock, R. C. Pooser, D. J. Dean, and P. Lougovski, *Physical Review Letters* **120**, 210501 (2018).
 - [6] O. Shehab, K. Landsman, Y. Nam, D. Zhu, N. M. Linke, M. Keesan, R. C. Pooser, and C. Monroe, *Physical Review A* **100**, 062319 (2019).
 - [7] D. Maslov, Y. Nam, and J. Kim, *Proceedings of the IEEE* **107**, 5 (2019).
 - [8] E. National Academies of Sciences and Medicine, *Quantum Computing: Progress and Prospects*, edited by E. Grumbling and M. Horowitz (The National Academies Press, Washington, DC, 2019).
 - [9] R. P. Feynman, *International Journal of Theoretical Physics* **21**, 467 (1982).
 - [10] S. Lloyd, *Science* **273**, 1073 (1996).
 - [11] A. Peruzzo, J. McClean, P. Shadbolt, M.-H. Yung, X.-Q. Zhou, P. J. Love, A. Aspuru-Guzik, and J. L. O’Brien, *Nature Communications* **5**, 4213 (2014).

- [12] A. M. Childs, D. Maslov, Y. Nam, N. J. Ross, and Y. Su, Proceedings of the National Academy of Sciences **115**, 9456 (2018).
- [13] J. D. Whitfield, J. Biamonte, and A. Aspuru-Guzik, Molecular Physics **109**, 735 (2011).
- [14] A. Bocharov, M. Roetteler, and K. M. Svore, Physical Review Letters **114**, 080502 (2015).
- [15] P. Jordan and E. Wigner, Zeitschrift für Physik **47**, 631 (1928).
- [16] S. B. Bravyi and A. Y. Kitaev, Annals of Physics **298**, 210 (2002).
- [17] M. Steudtner and S. Wehner, New Journal of Physics **20**, 063010 (2018).
- [18] G. H. Low and I. L. Chuang, Quantum **3**, 163 (2019).
- [19] G. H. Low and I. L. Chuang, Physical Review Letters **118**, 010501 (2017).
- [20] D. W. Berry, G. Ahokas, R. Cleve, and B. C. Sanders, Communications in Mathematical Physics **270**, 359 (2007).
- [21] M. R. Hoffmann and J. Simons, The Journal of Chemical Physics **88**, 993 (1988).
- [22] R. J. Bartlett, S. A. Kucharski, and J. Noga, Chemical Physics Letters **155**, 133 (1989).
- [23] M. Suzuki, Journal of Mathematical Physics **32**, 400 (1991).
- [24] Y. Nam, N. J. Ross, Y. Su, A. M. Childs, and D. Maslov, npj Quantum Information **4**, 23 (2018).
- [25] D. Maslov, Physical Review A **93**, 022311 (2016).
- [26] J. I. Cirac and P. Zoller, Physical Review Letters **74**, 4091 (1995).
- [27] D. Maslov and Y. Nam, New Journal of Physics **20**, 033018 (2018).
- [28] J. Romero, R. Babbush, J. R. McClean, C. Hempel, P. J. Love, and A. Aspuru-Guzik, Quantum Science and Technology **4**, 014008 (2018).
- [29] R. M. Parrish, L. A. Burns, D. G. A. Smith, A. C. Simmonett, A. E. DePrince, E. G. Hohenstein, U. Bozkaya, A. Y. Sokolov, R. Di Remigio, R. M. Richard, J. F. Gonthier, A. M. James, H. R. McAlexander, A. Kumar, M. Saitow, X. Wang, B. P. Pritchard, P. Verma, H. F. Schaefer, K. Patkowski, R. A. King, E. F. Valeev, F. A. Evangelista, J. M. Turney, T. D. Crawford, and C. D. Sherrill, Journal of Chemical Theory and Computation **13**, 3185 (2017).
- [30] J. T. Seeley, M. J. Richard, and P. J. Love, The Journal of Chemical Physics **137**, 224109 (2012).
- [31] K. N. Patel, I. L. Markov, and J. P. Hayes, Quantum Information and Computation **8**, 282294 (2008).
- [32] K. Raghavachari, G. W. Trucks, J. A. Pople, and M. Head-Gordon, Chemical Physics Letters **157**, 479 (1989).
- [33] Y. S. Lee, S. A. Kucharski, and R. J. Bartlett, The Journal of Chemical Physics **81**, 5906 (1984).
- [34] M. Urban, J. Noga, S. J. Cole, and R. J. Bartlett, The Journal of Chemical Physics **83**, 4041 (1985).
- [35] P. Gokhale, O. Angiuli, Y. Ding, K. Gui, T. Tomesh, M. Suchara, M. Martonosi, and F. T. Chong, arXiv preprint arXiv:1907.13623 (2019).

SUPPLEMENTARY MATERIAL

S1. FERMIONIC LEVEL LABELING

Each one- and two- body operators contain two and four indices, respectively. The specific numerical values of these indices are arbitrary. Note that the Pauli strings for the excitation

operator, after applying the fermion \mapsto qubit transformation of choice, have a dependence on the index values according to (16). We may thus use the label degree of freedom to reduce the number of two-qubit gates required to implement the one- and two-body Trotter terms, since fewer Pauli matrices in a given Pauli string leads to a smaller number of two-qubit gates.

Exploring all possible permutations is computationally prohibitively expensive as the total number of permutations is $n!$, where n is the total number of labels. We thus resort to a simple greedy approach. Specifically,

1. *Initialization of permutation matrix P and labelling L_0 :* We generate an array of permutation matrices P for all possible k -index switches. In total there are nP_k possible permutations. In our implementation, we used $k = 2$. Let us denote the initial fermion labels as L_0 . We compute the number of two-qubit gates that corresponds to each of relabeling $P_i L_0$ by simply adding the number of CNOT gates required for each excitation term obtained from the intra-Trotter term reordering subroutine.
2. *Iteration and termination criteria:* Denoting the current m^{th} generation labeling as L_m , we decide the next labelling by comparing each of $P_i L_m, i \in [0, {}^nP_k)$. If there is no $L_{m'} = P_i L_m$ that results in a lower CNOT count than L_m , we terminate the process and return L_m as the optimal labelling. Otherwise, we pick P_j which results in the lowest number of CNOTs, and continue the iterative process with the new labeling $L_{m+1} = P_j L_m$.

We note that once the final labels are determined, they are applied to all relevant fermionic operators, including the molecular Hamiltonian, to be consistent throughout our simulation.

S2. INTRA-TROTTER TERM ORDERING

We start by briefly noting that each one-body term leads to only one ordering, up to inversion. This is so, because it contains only two Pauli strings. Therefore, the one-body term does not require a specific ordering.

We next consider two-body operators. A single two-body operator, after applying proper transformation and PF algorithm, contains eight subterms. Specifically, we have

$$U^{\text{two-body}} \approx \prod_{j=0}^7 e^{-i\theta \otimes_v \sigma^{(j,v)}/2}, \quad (\text{S1})$$

where j denotes the intra-Trotter term index, v denotes the qubit index, $\sigma \in \{\mathbf{1}, \sigma_x, \sigma_y, \sigma_z\}$, and the approximation sign is due to the PF algorithmic errors. Each of the intra-Trotter term $e^{-i\theta \otimes_v \sigma^{(j,v)}/2}$ can be readily translated into a standard circuit as described in Eq. (8) in Section Methods H of [4]. In a naive implementation of U that uses an arbitrary fermion to qubit transformation, each intra-Trotter term results in $2(N_j - 1)$ number of CNOT gates, where N_j is the number of non-identity $\sigma^{(j,v)}$ in the j^{th} Pauli string.

Compared to the JW transformation, in the GT method, it is useful to have a more concrete set of rules to determine which qubit may be used as a target qubit t , in relation to the realization of U as a quantum circuit (see, e.g., Eq. 8 (b) in Section Methods H of [4], for the JW transformation). In the JW transformation, any choice of t such that $\sigma^{(j,t)}$ are either σ_x or σ_y , i.e., the qubits that correspond to the fermion labels in the two-body term,

are good choices. However, if $\sigma^{(j,t)} = \mathbf{1}$ in any one of the eight Pauli strings in U above, which frequently occur in the GT method, the intended target qubit index t is unusable. Therefore, in the GT method, qubit choices t that lead to $\sigma^{(j,t)} = \mathbf{1}$ are removed from the set of eligible targets that start with all qubits that correspond to the fermion labels that appear in the two-body term of interest and will subsequently not be used in the inter-Trotter term reordering subroutine detailed in Sec. S3.

Now, for a chosen target qubit of choice t , we consider the ordering of intra-Trotter terms to maximize the CNOT reduction. In particular, we only consider the CNOT reduction between adjacent Pauli string circuits. For each of adjacent intra-Trotter terms, i.e., $e^{-i\frac{\theta}{2}\otimes_v\sigma^{(j,v)}}$ and $e^{-i\frac{\theta'}{2}\otimes_v\sigma^{(j+1,v)}}$, where $j \in [0, 6]$, we enumerate v through all non-target qubits. We then compare $\sigma^{(j,v)}$ and $\sigma^{(j+1,v)}$. For a particular control qubit v , if neither of the two aforementioned Pauli matrices $\sigma^{(j,v)}$ and $\sigma^{(j+1,v)}$ are $\mathbf{1}$, then the circuit can be expressed as Fig. S1. In this particular circuit, if we have $M_0 = M_2$, there is a two CNOT reduction, while, if we have $M_0 \neq M_2$, there is a one CNOT reduction, according to the circuit identity discussed in [4] Method H. Suppose now there are $m_j^{(t)}$ two-CNOT reductions and $n_j^{(t)}$ one-CNOT reductions for the chosen target qubit t . Then, the total number of CNOT reduction is $2m_j^{(t)} + n_j^{(t)}$ for the target qubit of choice t . The total optimized number of CNOTs for a chosen target t of a certain ordering is thus $N^{(t)} = \sum_{j=0}^7 2(N_j - 1) - \sum_{j=0}^6 (2m_j^{(t)} + n_j^{(t)})$.

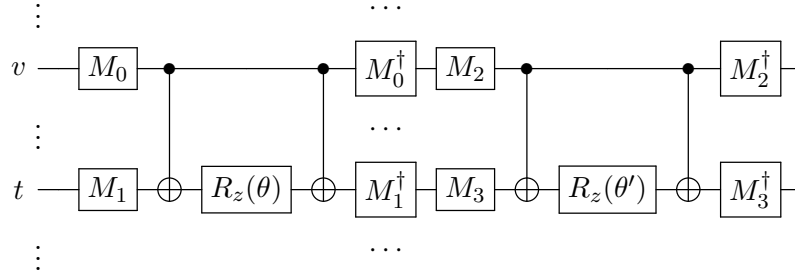


FIG. S1. Example circuit for adjacent Pauli string circuits $e^{-i\frac{\theta}{2}\sigma_0^v\otimes\sigma_1^t\otimes\cdots}e^{-i\frac{\theta'}{2}\sigma_2^v\otimes\sigma_3^t\otimes\cdots}$. Subscripts j to Pauli operators are introduced to conveniently label the associated operators M_j shown in the figure. t denotes the target qubit, v denotes the control qubit, $\sigma_j \in \{\sigma_x, \sigma_y, \sigma_z\}$, and $M_j \in \{\mathbf{H}, \mathbf{s}^\dagger\mathbf{H}, \mathbf{1}\}$. If $\sigma_j = \sigma_x$, $M_j = \mathbf{H}$. If $\sigma_j = \sigma_y$, $M_j = \mathbf{s}^\dagger\mathbf{H}$. If $\sigma_j = \sigma_z$, $M_j = \mathbf{1}$.

At this point, we are equipped to compute and compare $N^{(t)}$ among all possible orderings and all possible targets to determine which the target qubit set and the intra-Trotter ordering result in the minimum number of CNOTs. We note that for a certain ordering, there likely is a degeneracy in the choice of target qubit t that results in the same CNOT counts. All of these degenerate cases with the optimal resources are returned to the Inter-Trotter term ordering routine, detailed in Sec. S3, for use.

S3. INTER-TROTTER TERM ORDERING

In this subroutine, we first run a preprocessing step based on the information passed from the intra-Trotter term optimization step described in Sec. S2. Specifically, for operators $a_i^\dagger a_j$ and $a_i^\dagger a_j^\dagger a_k a_l$, we check if any one of the indices i and j for the former, and i, j, k , and l for the latter, may or may not be used as a target qubit in the circuit implementation of the

operators in the standard compilation (see, e.g., Fig. 2d of [4] for a two-body term using the JW transformation). See Sec. S2 for details. We flag the qubit indices that cannot be used as a target as ineligible.

After all of the ineligibilities have been determined, we proceed according to a simple greedy approach. We first identify the most frequently eligible index, say p , across all terms. Then, we group all terms with the index p as an eligible target qubit and classify them under the equivalence class $[p]$. We next remove all the group elements from the list of one- and two-body operators. We repeat the procedure from the identification of the most frequent eligible index until no more operators are left in the list.

Note that the quantum resource cost reduction will likely now result in between the circuit representation of the elements of the same equivalence class, since the target qubit of two-qubit gates from each element of the same class is the same. Therefore, once all of the equivalence classes are specified, we consider permuting the orderings by which the elements are implemented on a quantum circuit. Considering all permutations can be prohibitively expensive. We thus use a simple greedy approach once more, first starting out with two of the elements that result in the most resource cost reduction. Then, we concatenate a next element, identified from the set of elements that have not been implemented in the circuit, based on the resource cost reduction. We repeat the concatenation process until no more element is left in the set. We note that each trial of testing out which element may be the best for the given iteration consists in general of four cases. This is so, since the circuit concatenation may be performed as a prefix or suffix, and the element to be concatenated can be considered in its original intra-term order or the reverse.

S4. GENERALIZED BOSONIC TERM

The correspondence between Generalized Bosonic terms and Fermionic terms can be established as follows. A Fermionic double excitation term $\theta_{pqrs}(a_p^\dagger a_q^\dagger a_r a_s - h.c.)$, when transformed by the JW transformation, turns into $\theta_{pqrs}(\sigma_+^p \sigma_+^q \sigma_-^r \sigma_-^s \otimes_k \sigma_z^k - h.c.)$. If p and q belong to the same spatial orbital and r and s belong to yet another same spatial orbital, assuming no other terms that break the symmetry between p and q or r and s have been considered in the circuit, p and q levels may be encoded by a single qubit and likewise for the r and s levels. In this case, using p and r as representatives, the qubit-space operator can be simplified to $\theta_{pqrs}(\sigma_+^p \sigma_-^r \otimes_{k'} \sigma_z^{k'} - h.c.)$, where k' runs over the set of qubits σ_z operator needs to be applied for the given excitation term in the appropriately reduced space. The appropriately reduced space may include the single qubits that each denotes the reduced, symmetric levels and those that are not reduced. To illustrate, if two of the levels k_1 and k_2 in the original space require σ_z and if k_1 and k_2 are encoded into a single index k' , we simply call $\sigma_z^{k'}$ twice, one each for k_1 and k_2 . This for instance amounts to identity, which results in resource savings.

S5. ROUTINE: β OPTIMIZATION

For the β optimization, we used particle swarm optimization method. To describe the process, we introduce the three-index notation for our β matrix particle. Specifically, we use $\beta(i, j, m)$, where i is the index for walker, j is the step for walker i , and m is the possible direction for walker i at step j . $j = 0$ denotes the initial step of walker i . $m = 0$ denotes

the current optimal direction for walker i at step j . We detail the steps in the following.

- Step 1: Walker initialization:** Randomly initialize k different $\beta(i, 0, 0)$ matrix where $i = 1, 2, \dots, k$ (see Sec. S6). Each $\beta(i, 0, 0)$ matrix can be regarded as a walker and evolved independently. The reference value of the current, j th step is the cost function $f(\beta(i, j, 0))$, such as the number of two-qubit gates of the optimized quantum circuit, as was used in section IV B.
- Step 2: Propagate walkers:** For each of the walker i , at step $j(\geq 0)$, generate a new matrix $\beta(i, j, m)$ that has Hamming distance 1 from $\beta(i, j, 0)$. Non-invertible binary matrices are automatically skipped. The index $m \in [0, n(n-1)/2]$, where n is the number of qubits, denotes the potentially non-zero binary matrix entry, where the bit value does not agree between $\beta(i, j, 0)$ and $\beta(i, j, m)$.
- Step 3: Termination criteria:** For a certain walker i , at step j , obtain the cost function $f(\beta(i, j, m))$ for all new matrices generated in step 2. Compare $f(\beta(i, j, m))$ for all m and pick the m' that returns the minimal number of CNOT gates. If $m' \neq 0$ and $f(\beta(i, j, m')) < f(\beta(i, j, 0))$, set $\beta(i, j+1, 0)$ as $\beta(i, j, m')$ and continue with the optimization process with the walker i . Otherwise, terminate the propagation of the walker.
- Step 4: Local minimum:** After the termination of all walkers, determine the walker i' with the minimal cost $f(\beta(i', j', 0))$. The locally optimal β is $\beta(i', j', 0)$.

S6. β MATRIX INITIALIZATION

It is seemingly impossible to sample sufficient number of β matrices, especially as the number of qubits increases. Thus, any insight as to how to choose such a matrix will be helpful. As one of the examples, we study the correlation between the number of ones in our upper triangular β matrix (sparsity) and the number of CNOTs it produces. The system we used as an example is the water molecule in STO-3G basis with 21 excitation terms, as used in Table II of the main text. To explore the large space of possible β , we randomly sampled the β matrix space for a fixed number of ones in the potentially non-zero entries of the matrix. The best result for each of the fixed number of ones is shown in Fig. S2.

As can be seen from Fig. S2, it is clear that a better transformation is more likely to be found to be a sparse matrix, similar to the JW transformation, i.e., an identity matrix. There are only a few points that have a lower number of CNOT counts than the JW transformation. Closely examining these matrices, we found that the matrices that require fewer CNOTs than the JW transformation are all sparse with only a few entries populated by one in the non-main diagonal. In addition, we found that most of these matrices have one non-zero entry in the first diagonal above the main diagonal.

Taking this observation into consideration, we can design a rule to populate sample initial walkers containing only one entry in the first diagonal above the main diagonal being one, otherwise the same as the JW transformation. Each walker will gradually evolve according to the algorithm specified in Sec. S5. This has an additional benefit that the initial number of walker is now only $n - 1$, where n is the number qubits of the system.

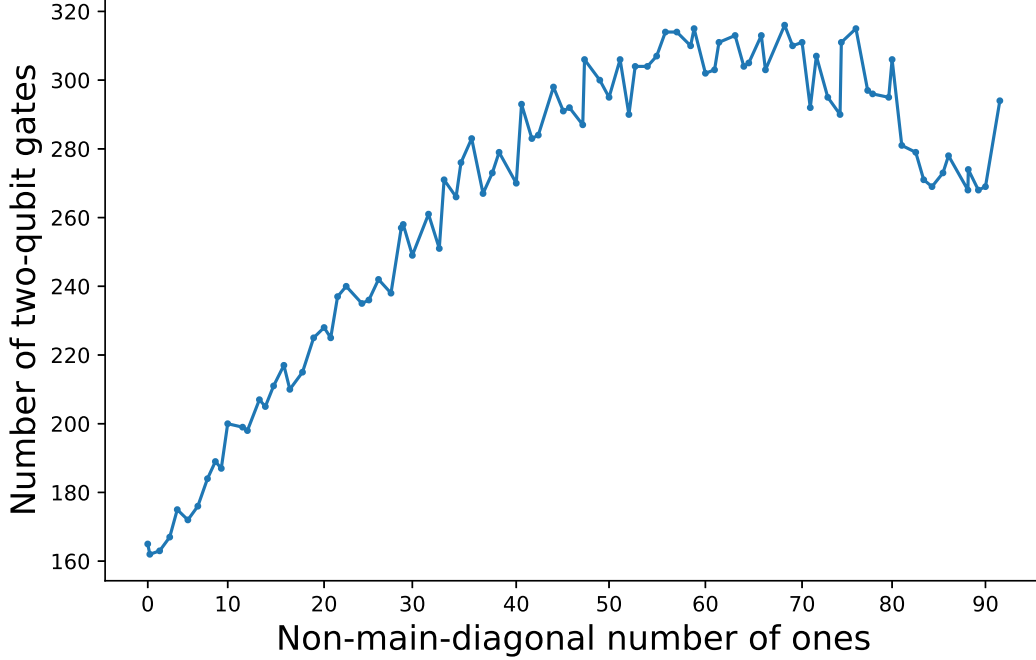


FIG. S2. Number of two-qubit gates as a function of the non-main-diagonal number of ones in the β matrix. We plot the minimal number of two-qubit gates found for each sample β matrices generated for a fixed number of ones in the non-main diagonal. As a concrete example, we considered the specific case of $\text{H}_2\text{O}(21)$ in Table II of the main text. With the exception of the cases with the number of non-main-diagonal ones being 1, 2, 90, and 91, we sampled at least 200 times (roughly of about 300 times on average) per each non-main-diagonal number of ones. For the case with 1 and 91 non-main-diagonal ones, we sampled the only possible, single case. For the case with 2 and 90 non-main-diagonal ones, we sampled all possible 91 cases.

S7. REDUCTION OF PAULI STRING MEASUREMENT

For a given UCC ansatz and the Pauli strings to be measured for their expectation-value evaluations, naively, one could in principle consider each individual strings separately. However, considering each strings one at a time could be a challenging task. Thus, we attempt to reduce the number of measurements we need to consider using the following two methods.

1. *Filter out non-contributing Pauli strings:* Consider $|\Psi_{\text{UCC}}\rangle = \sum_i c_i |i\rangle$. Consider further the expectation value of a Pauli string $\otimes_v \sigma^v$, i.e.,

$$\begin{aligned} \langle \Psi_{\text{UCC}} | \otimes_v \sigma^v | \Psi_{\text{UCC}} \rangle &= \left(\sum_i c_i^* \langle i | \right) \otimes_v \sigma^v \left(\sum_k c_k |k\rangle \right) \\ &= \sum_{i,k} c_i^* c_k \langle i | \otimes_v \sigma^v |k\rangle \end{aligned} \tag{S2}$$

where $\sigma^v \in \{\mathbf{1}, \sigma_x, \sigma_y, \sigma_z\}$ is the Pauli operator for v th qubit. For a fixed i and k , if $\langle i | \otimes_v \sigma^v | k \rangle = 0$ or $c_i^* c_k = 0$, the product of the two does not contribute to the sum in (S2). This implies that, if one can determine that the amplitudes c_i or c_k must be zero (or sufficiently small, given some target simulation accuracy) for all non-zero $\langle i | \otimes_v \sigma^v | k \rangle$, either by the structure of the circuit that prepares $|\Psi_{\text{UCC}}\rangle$ or by the measurement of $|\Psi_{\text{UCC}}\rangle$ itself in its computational basis, in principle, one may evaluate the expectation value in (S2) to be zero without performing explicit measurements targeted specifically for the given Pauli string. We refer to this process of determining whether a Pauli string can be safely disregarded or not as the screening process. This screening process, applied to a set of Pauli strings that need to be measured for our VQE approach, works effectively if $|\Psi_{\text{UCC}}\rangle$ has a tractable number of non-zero components.

2. Measure Pauli strings simultaneously:

To avoid introducing additional two-qubit gates that may be required to measure all commuting Pauli strings simultaneously [35], we decided to use the qubit-wise commutation based method, also used in [4], to reduce the total number of measurements. Specifically, we start with a common basis that is initialized based on the first Pauli string, $\otimes_v \sigma^{v,1}$, of our choice. Then, the second Pauli string $\otimes_v \sigma^{v,2}$ can be measured together with the common basis, if for each v , $\sigma^{v,1} = \sigma^{v,2}$ or $\sigma^{v,1} = \mathbf{1}$ or $\sigma^{v,2} = \mathbf{1}$. If $\sigma^{v,1} = \mathbf{1}$ and $\sigma^{v,2} \neq \mathbf{1}$, we update $\sigma^{v,1} = \sigma^{v,2}$ and continue until no further Pauli strings can be measured using the common basis. We group the identified Pauli strings that can be measured with the common basis, represented by the final $\otimes_v \sigma^{v,1}$, and remove them from the list of Pauli strings. We iterate this process until there is no Pauli string is left in the list. The total number of measurements that we need to consider then is the number of common bases considered in this iteration process.